WPS8188

Policy Research Working Paper 8188

Natural Disaster Damage Indices Based on Remotely Sensed Data

An Application to Indonesia

Emmanuel Skoufias
Eric Strobl
Thomas Tveit

WORLD BANK GROUP
Poverty and Equity Global Practice Group
September 2017

Policy Research Working Paper 8188

Abstract

Combining nightlight data as a proxy for economic activity with remote sensing data typically used for natural hazard modeling, this paper constructs novel damage indices at the district level for Indonesia, for different disaster events such as floods, earthquakes, volcanic eruptions and the 2004 Christmas Tsunami. Ex ante, prior to the incidence of a disaster, district-level damage indices could be used to determine the size of the annual fiscal transfers from the central government to the subnational governments. Ex post, or after the incidence of a natural disaster, damage indices are useful for quickly assessing and estimating the damages caused and are especially useful for central and local governments, emergency services, and aid workers so that they can respond efficiently and deploy resources where they are most needed.

This paper is a product of the Poverty and Equity Global Practice Group. It is part of a larger effort by the World Bank to provide open access to its research and make a contribution to development policy discussions around the world. Policy Research Working Papers are also posted on the Web at http://econ.worldbank.org. The authors may be contacted at eskoufias@worldbank.org.

Natural Disaster Damage Indices Based on Remotely Sensed Data: An Application to Indonesia*

Emmanuel Skoufias (World Bank)
Eric Strobl (University of Bern)
Thomas Tveit (University of Cergy-Pontoise)

JEL Classification: Q54, C63, R11, R5,O18
Keywords: Remotely Sensed Data, Natural Disasters, Natural Hazard model, Damage Index, Floods, Earthquakes, Volcanic Eruptions

*This paper was financed in part by the Disaster Risk Finance Impact Analytics project of the Disaster Risk Financing and Insurance Program of The World Bank Group

1 Introduction

Quickly assessing and estimating the damage caused after the incidence of a natural disaster is important for both central and local governments, emergency services and aid workers, so that they can respond efficiently and deploy resources where they are most needed. Recently, remote sensing technologies have been used to analyze the impact of disasters, such as hurricanes (Myint *et al.*, 2008; Klemas, 2009), floods (Haq *et al.*, 2012; Wu *et al.*, 2012, 2014; Chung *et al.*, 2015), landslides (Nichol *et al.*, 2006), earthquakes (Fu *et al.*, 2005; Yamazaki & Matsuoka, 2007), wildfires (Holden *et al.*, 2005; Roy *et al.*, 2006), volcanoes (Carn *et al.*, 2009; Ferguson *et al.*, 2010) and tsunamis (Römer *et al.*, 2012). These remote sensing techniques are useful for providing quick damage estimates shortly after the disasters giving emergency services a chance to respond quickly and local governments an overview of estimated costs and necessary repairs.

In addition to their usefulness in the aftermath of a disaster, estimates of the potential damage associated with a natural disaster are also useful for policy making prior to the realization of the natural hazard event. In many cases the incidence of a natural hazard event can turn into a natural disaster simply because of inadequate preparation ex-ante. Indonesia, for example, is highly exposed to natural disasters by being situated in one of the worlds most active disaster hot spots, where several types of disasters such as earthquakes, tsunamis, volcanic eruptions, floods, landslides, droughts and forest fires frequently occur. The average annual cost of natural disasters, over the last 10 years, is estimated at 0.3 percent of Indonesian GDP, although the economic impact of such disasters is generally much higher at local or subnational levels (The Global Facility for Disaster Reduction and Recovery, 2011). The high frequency of disasters experienced has important impacts on expenditures by local governments that could be anticipated, at least in part, through upward adjustments in the annual fiscal transfers from the central government to the subnational governments.[1] Such ex-ante adjustments in the level of fiscal transfers would be more useful if they could be based on estimates of the potential damages associated with the incidence of a natural disaster as opposed to estimates of the intensity of the potential natural hazard that might occur. However, although in recent years there has been much progress towards the modeling of the main natural hazards, there continues to be a scarcity of estimates of the damages associated with the incidence of these disasters. The value of damage caused by a natural disaster is typically a complicated function of the size of population living in that area, the level and type of economic activity carried out, the value of the physical infrastructure in place, and the resilience of infrastructure and people's livelihoods to the natural hazards.

This paper fills some of the gaps in the literature by using different remote sensing sources and data on the physical characteristics of the events to construct four damage indices for natural disasters in Indonesia. The indices cover floods, earthquakes, volcanic eruptions and a tsunami, and are all weighted by local economic activity in an area, and then aggregated up to a district level.[2] All data used in the construction of the indices are free and publicly available, making the methods used a potentially very useful alternative for both central and local governments to quickly get a rough estimate of the damages caused by a disaster (either ex-ante or ex-post).[3]

Importantly, all of the indices constructed take into account local exposure. Given limited access to highly disaggregated local economic activity data, nightlight intensity derived from satellite imagery has proved to be a good proxy; see, for instance, Henderson *et al.* (2012), Hodler & Raschky (2014) and Michalopoulos & Papaioannou (2014). By utilizing the grid cells of approximately 1 square kilometer we can break down areas in cities and districts into where they are busiest, and thus take into account not only the local physical characteristics of a natural disaster but also the local economic activity exposed to it.

The paper is structured as follows. Section 2 of the paper discusses in more detail the incidence and types of natural disasters. Section 3 discusses the nightlights data. Sections 4-7 discuss in detail the construction of the four damage indices, while section 8 concludes.

[1] For example, Indonesia experienced 4,000 disasters between 2001 and 2007 alone, including floods (37%), droughts (24%), landslides (11%) and windstorms (9%) (The Global Facility for Disaster Reduction and Recovery, 2011).

[2] A tropical cyclone index was also constructed, but no hurricanes had strong enough winds to cause any damage on land.

[3] In a separate paper, Skoufias *et al.* (2017), we correlate the damage indices of these disasters at the district level with the ex-post allocation of district expenditures in different sectors and by economic classification.

2 Natural Disasters in Indonesia

Natural disasters are prevalent events across most parts of Indonesia. According to the Indonesian National Disaster Management Authority (BNPB) there were more than 19,000 natural disasters in the period 2001 - 2015 (National Disaster Management Agency, BNPB, 2016), making Indonesia a useful country for any natural disaster analysis. The most frequent disasters are floods and landslides (52 percent), strong winds (21 percent) and fires (15 percent), while the most damaging ones are earthquakes, tsunamis and volcanic eruptions, which all cause major damage to buildings and infrastructure in addition to the human casualties. The deadliest year according to the BNPB data was 2004, where there were more than 167,000 deaths due to natural disasters and 166,671 of them stemming from the tsunami in December 2004.

2.1 Floods

The tropical climate of Indonesia often leads to annual floods. The BNPB data registered more than 10,000 incidents of floods or landslides leading to more than 3,500 fatalities from 2001 through 2015. During the period from 1985 to 2016, The Darthmouth Flood Observatory (DFO) registered 3,808 floods of magnitude 4 or more and 1,175 floods of magnitude 6 and up.[4] Of these floods, there were 126 large scale floods with a centroid within Indonesia in the period from 2001 to 2016 as can be seen in Figure 1. Of the 34 provinces, 27 experienced having a centroid of a large scale flood event during these years.[5]

Figure 1: DFO Large Scale Floods in Indonesia 2001-2016

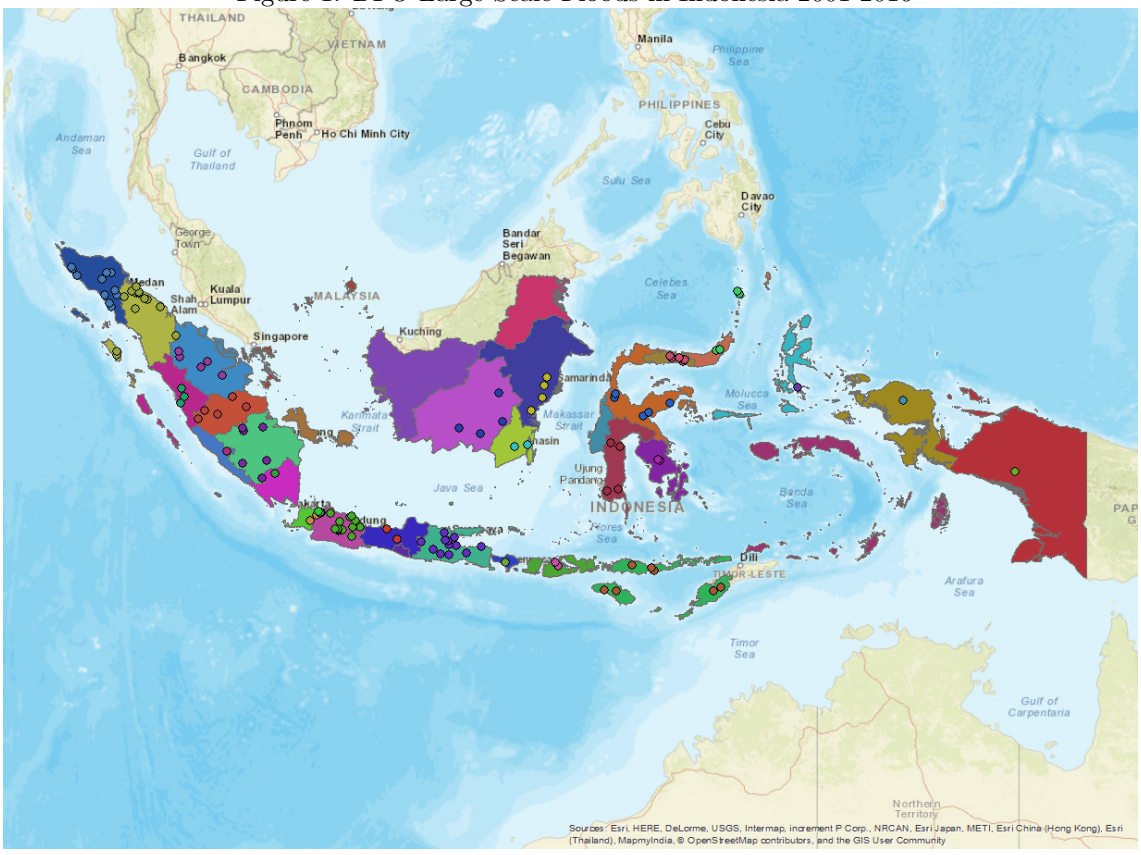

Source: G.R.Brakenridge (2016)

[4]Magnitude is defined as: $M = \log(D * S * AA)$, where D is the duration of the flood; S is the severity on a scale consisting of 1 (large event), 1.5 (very large event) and 2 (extreme event); and AA is the size of the affected area. Flood events registered by DFO have mainly been derived from news and governmental sources.

[5]The provinces where no large scale centroid was present were Bangka Belitung, Riau Islands, Kalimantan Barat, Yogyakarta, Sulawesi Barat, Kalimantan Utara and Maluku. Note that some of these, like Kalimantan Utara, Kalimantan Barat, Sulawesi Barat and Yogakarta, did most likely experience large scale flood during these years, but that the centroid was in another province. The remaining three provinces consist mainly of smaller islands, so the flooded area will most likely not constitute a large scale flood event.

2.2 Earthquakes

Due to Indonesia's location inside the Pacific Ring of Fire, one of the most seismically active areas in the world, it is often struck by earthquakes. BNPB counted almost 400 earthquakes from 2001 to 2015, with the largest number of casualties coming from the tsunami created by a 9.0 earthquake located off the coast of Aceh, otherwise known as the earthquake that caused the 2004 tsunami. Apart from that, there were more than 8,000 registered fatalities due to earthquakes over the same period. Overall, this makes earthquakes the deadliest of the natural disasters that strike Indonesia.

Figure 2 shows how common earthquakes are in Indonesia by displaying contour maps[6] of all earthquakes of magnitude 5.0 and above that struck Indonesia from 2004 through 2014. In total, the United States Geological Survey (USGS) registered 261 earthquakes.[7]

Figure 2: Earthquakes in Indonesia 2004-2014

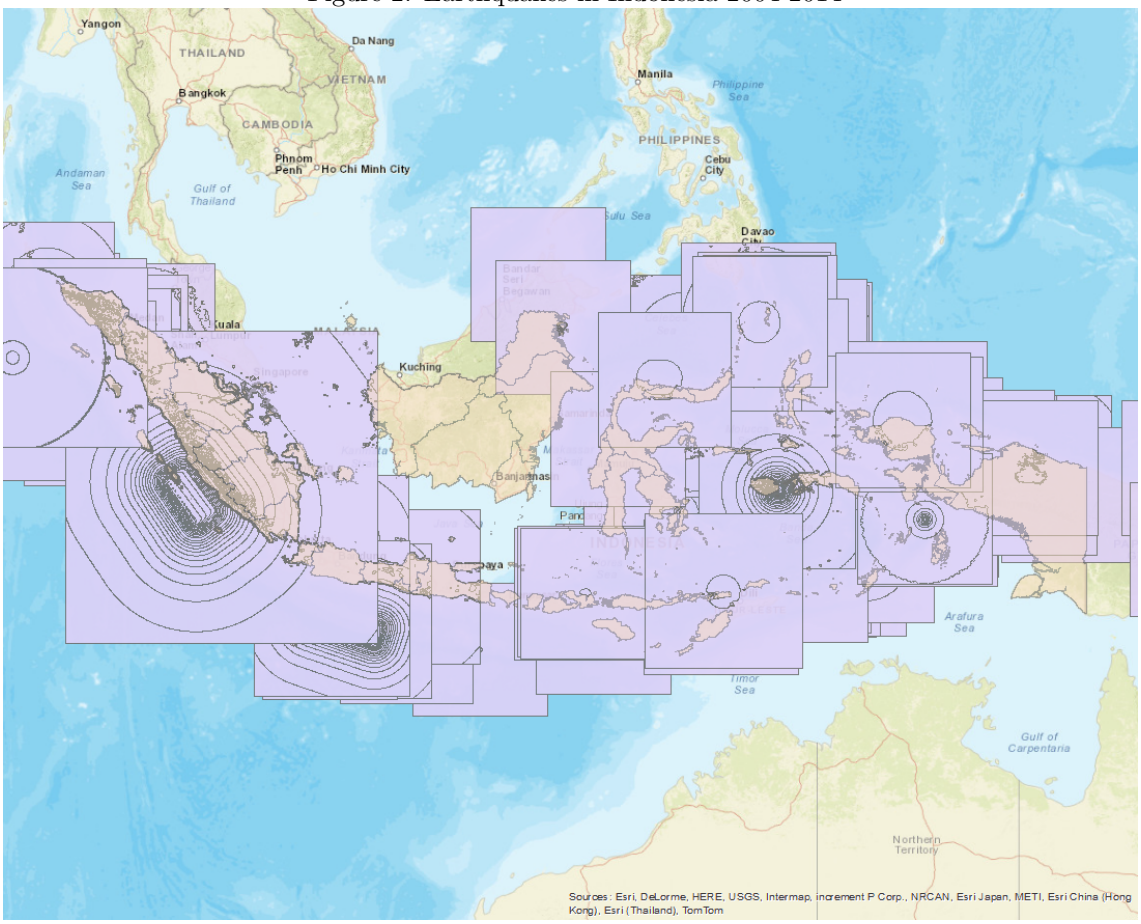

Source: USGS

2.3 Volcanic activity

Indonesia has the highest number of active volcanoes in the world, numbering almost 150. Of these, many have had eruptions in both more historical times and after the year 2000. The most famous eruption is probably the explosion of Krakatau in August 1883, when two-thirds of the Krakatau Island erupted and disappeared, killing more than 35,000 people and causing a global mini ice age and weather disruptions for years. BNPB have registered 92 eruptions over our 15-year time period and more than 60 major volcanoes that have had eruptions since 1900. The most recent one is the 2010 Mount Merapi eruption

[6] These maps are also known as ShakeMaps, which are produced by USGS.

[7] There are 1,002 earthquakes registered by USGS that were of magnitude 5.0 or more that had a point with a PGA of at least 0.05 within Indonesia. Many of these points create little to no damage. The 261 earthquakes mentioned above are quakes that are mostly contained within Indonesia.

that killed 324 people and dislocated more than 320,000.

In addition to the BNPB data, during the years 2004 through 2015 the Darwin Volcanic Ash Advisory Centre (DVAAC) had 587 days where they issued a red warning, implying an ongoing or imminent volcanic eruption. The most active volcanoes - measured by number of days with red warnings - are shown in Table 1, with the top 5 volcanoes constituting almost 75 percent of the red warnings. These are also volcanoes that have been in the media, with Merapi already mentioned and Sinabung, which had several eruptions in 2010, 2013 and 2014. These two volcanoes are located close to densely populated areas, with Sinabung located in North Sumatra and Merapi in central Java.

Table 1: Most Active Volcanoes 2004-2015

Volcano	Number of Days with Red Warning
Sinabung	224
Merapi	92
Manam	74
Egon	36
Soputan	31

2.4 2004 Christmas Tsunami

The Christmas Tsunami in 2004 is the worst singular natural disaster during the modeling period, and one of the worst natural disasters in world history. As seen in the photo in Figure 3 the destruction was absolute in parts of Indonesia. The total death toll across Indonesia and 13 other countries was more than 230,000 people and there were many more missing. In addition, the World Bank (2005) estimated a total economic impact of 4.5 billion US dollars. The official BNPB data for Indonesia estimates 166,671 deaths due to the tsunami.

The cause of the tsunami was an earthquake of magnitude 9.0 150 miles south-south east of Banda Aceh on the morning of 26 December. This quake created a tsunami with waves more than 20 meters high at the highest. Due to the fault line of the earthquake being in a north-south direction, the greatest strength of the tsunami was in an east-west direction (Athukorala & Resosudarmo, 2005). This led to the largest damages being in the northern part of Sumatra, in the province of Aceh, where entire villages were wiped out as seen in the photo of Banda Aceh (Figure 3).

Figure 3: Destruction in Banda Aceh

Source: The Atlantic (2014)

3 Nightlight Data

Natural disasters are inherent local phenomena in that they either affect only parts of areas and/or affect parts within areas differently. It is thus important to take the local population/asset exposure into account when constructing more aggregate proxies. Arguably one would like to have measures of exposure as spatially disaggregated as possible. For a country like Indonesia, data are usually sparse and at a very aggregated spatial level.

An alternative approach is thus to use nightlights as a proxy for local economic activity. As a matter of fact, nightlights have found widespread use where no other measures are available; see, for instance, Henderson *et al.* (2012), Hodler & Raschky (2014) and Michalopoulos & Papaioannou (2014). In Henderson *et al.* (2012), Indonesia is used as an example of using nightlights to capture an economic downturn following the Asian financial crisis in the late 1990s. Their results show that swings in GDP change can generally be captured. Nevertheless one has to account for factors such as cultural differences in light usage, latitude and gas flares. In our case this is unlikely to affect our results since we use nightlights to capture exposure within a country rather than across countries.

The nightlight imagery we employ is provided by the Defense Meteorological Satellite Program (DMSP) satellites. In terms of coverage each DMSP satellite has a 101 minute near-polar orbit at an altitude of about 800km above the surface of the earth, providing global coverage twice per day, at the same local time each day, with a spatial resolution of about 1km near the equator. The resulting images provide the percentage of nightlight occurrences for each pixel per year normalized across satellites to a scale ranging from 0 (no light) to 63 (maximum light). Yearly values were then constructed as simple averages across daily values of grids, and are available from 1992.[8] We use the stable, cloud-free series; see Elvidge *et al.* (1997).

The data revealed 414,644 cells which had a nightlight value greater than 0 in them at least once during the period 2001-2013. Figure 4 - containing all cells with nightlights in 2012 - shows that the large cities and densely populated areas on Java, Sunda Islands, coastal Kalimantan and Sumatra are fully covered in lights. Inner parts of Kalimantan and most parts of New Guinea are more sparsely lit.

Figure 4: Cells with Registered Nightlights in 2012

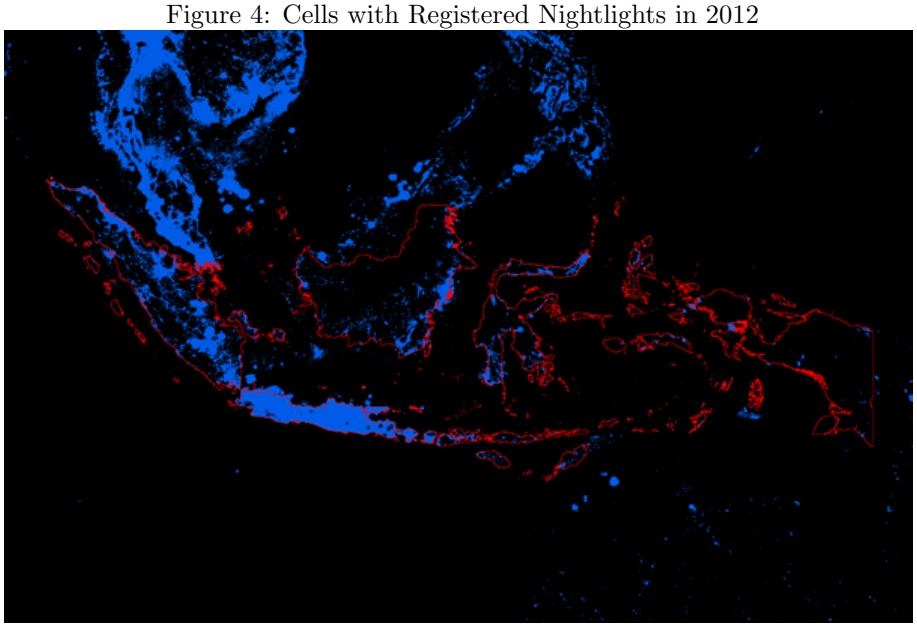

[8]For the years where satellites were replaced, DMSP provides an average from both the new and old satellite. In this paper we use the imagery from the most recent satellite but as part of our sensitivity analysis we also re-estimated our results using an average of the two satellites and the older satellite only. The results of these latter two options were almost quantitatively and qualitatively identical.

4 Flood Damage Index

The modeling of floods can be done by remote sensing (Brakenridge & Anderson, 2006; Wu *et al.*, 2012; Haq *et al.*, 2012) or through a combination of weather data and GIS systems as for example in Knebl *et al.* (2005); Asante *et al.* (2007); Dessu *et al.* (2016). We utilize the latter, as remote sensing is useful for assessing whether an area is flooded or not, but it is weaker on modeling the intensity of the flood. Moreover, cloud cover generally limits the accurate detection of floods from remote sensing sources.

To model floods we have decided to use the Geospatial Stream Flow Model (GeoSFM) which is a software that is "designed to use remotely sensed meteorological data in data sparse parts of the world"(Artan *et al.*, 2008). GeoSFM was developed by USGS and USAID and is a hydrological modeling tool used to model stream flows across large areas, in particular areas where highly localized data are lacking. It has been used in regions such as the Great Horn of Africa (Asante *et al.*, 2007; Mati *et al.*, 2008; Dessu *et al.*, 2016) and Nepal (Shrestha *et al.*, 2011), with Dessu *et al.* (2016) finding that the model captures 76% of the monthly average variability, making it useful for flood simulation.

The inputs needed to model stream flow for basins are soil- and terrain-based - such as digital elevations models (DEM) and land cover and soil data - and weather-based, such as precipitation and potential evapotranspiration (PET) data. The HYDRO1K data set from USGS, which is a DEM made for hydrological modeling based on the USGS' 30 arc-second DEM of the world, is used as elevation input. The land cover data are the Global Land Cover Characterization (GLCC) data set also from USGS, while the soil data are from the FAO Digital Soil Map of the World.

The daily precipitation data are from the 3-hourly data set from the Tropical Rainfall Measurement Mission Project (TRMM) and the PET data are 6-hourly data from the Global Data Assimilation System (GDAS), both data sets are aggregated up to daily data. The PET data are available from February 2001 and onwards, while the precipitation data are available for the period 1998-2014. Given that we only have nightlight data through 2013, we will focus on floods for the period 2001-2014.

GeoSFM uses the inputs to construct basins based on the terrain and then uses a linear soil moisture accounting routine to model surface runoff and soil moisture based on precipitation and PET. It is worth noting that although a more complex and better non-linear routine is also supported, it does not work well for our more generalized macro-modeling with fairly low resolution data. Finally, GeoSFM models the stream flow for each basin for each day of our time period.

Note that GeoSFM does not model coastal floods, nor does it model flash floods in areas where there are no rivers or streams of a certain length. Figure 5 shows that there are parts of Indonesia and even one province - Riau Islands - which have no basins. Another weakness is that it does not take into consideration the specific terrain within each basin. Floods are generally very localized events and the low resolution of our data makes it impossible to model the intensity of the stream flow within a basin and also causes some river outlets to be slightly inland instead of running all the way to the ocean.

4.1 Creation of Index and Results

The first part of constructing the index involves defining when a flood event is happening. In Wu *et al.* (2012) they propose four runoff based methods to define a flood threshold, and in addition Wu *et al.* (2014) propose a slightly modified flood threshold definition with a point being flooded when:

$$R > P_{95} + \sigma \qquad and \qquad Q > 10m^3/s \tag{1}$$

where R is the routed runoff in millimeters, P_{95} is the 95th percentile value and σ is the standard deviation of the routed runoff. Q is the discharge in cubic meters.

We found that with the GeoSFM modeled data, runoff was not a good proxy for flooding, due to it only capturing a limited number of floods. Discharge, Q, was a better proxy, leading to a new - but very similar - equation:

$$Q > P_{95} + \sigma \qquad and \qquad Q > 10m^3/s \tag{2}$$

Figure 5: Basins by Province

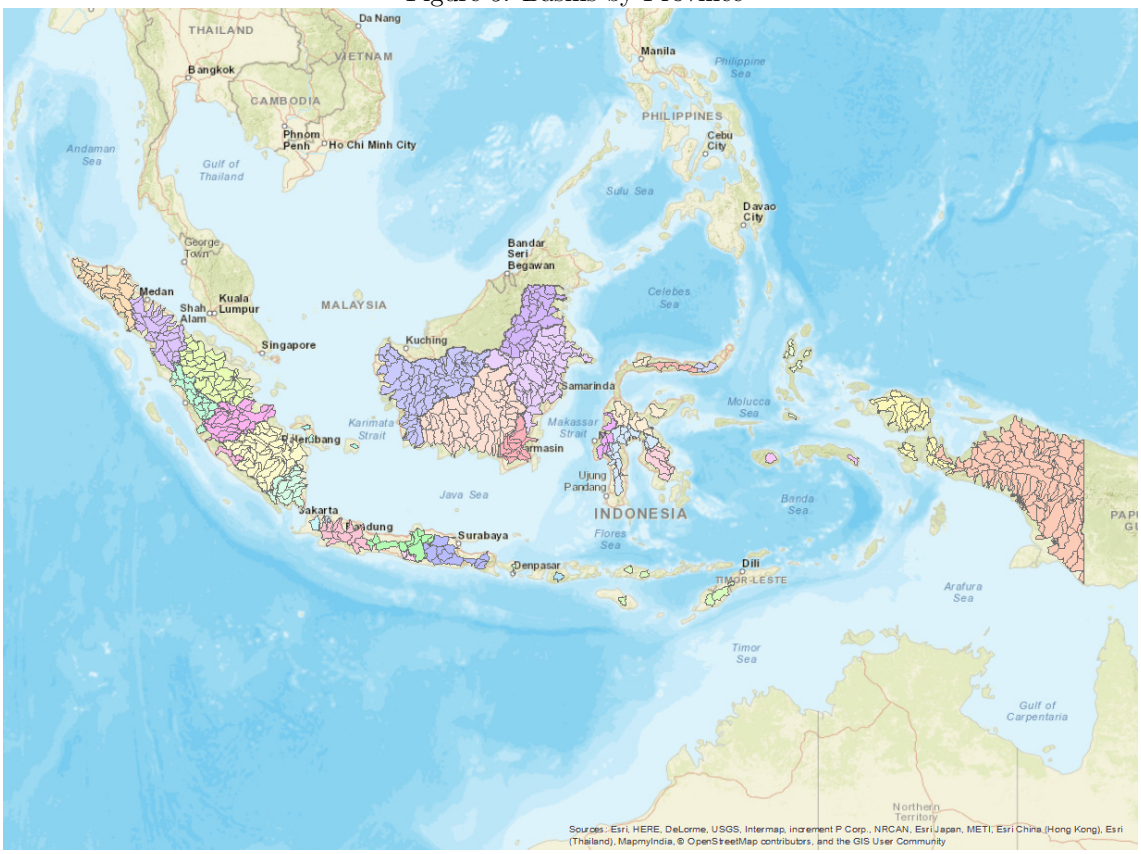

By manually checking against the DFO floods, we find that our data do hit several of the large scale events in Figure 1.

4.1.1 Damage Index

Due to floods being very localized, the modeling of damage is difficult, and no standard exists in the literature. Penning-Rowsell *et al.* (2005) base destruction on value of housing stock and the Standards of Protection and then uses an estimate of number of properties affected by different return period floods. Scawthorn *et al.* (2006) use a combination of building stock and velocity of the stream flow, whereas Kreibich *et al.* (2009) look at different parameters such as velocity, depth, energy head, stream flow and intensity. They find velocity to be a poor parameter for assessing damage, while water depth and energy head show the best results. Stream flow and intensity are also weak as parameters. Finally, Merz *et al.* (2010) assess different damage influencing parameters and point to the fact that most "damage influencing factors are neglected in damage modeling, since they are very heterogeneous in space and time, difficult to predict, and there is limited information on their (quantitative) effects". Overall, there is limited support in the literature for a strong correlation between these parameters and damages on anything but a very localized scale.

As for assessing the damage itself, Merz *et al.* (2010) discuss damage functions and the two main approaches, which involve one empirical approach where damage data are collected after the flood and one synthetic approach where they construct potential what if-scenarios. Once again the assessments rest on very localized data, which we do not have for Indonesia. Overall, it means that we cannot expect anything more than rough estimates. A common denominator for the papers mentioned above is that there is some measurement of intensity. Given that stream flow is an intensity proxy, we have used that to construct a simple measurement for intensity. The equation is:

$$I_{b,t} = \begin{cases} 0 & : Flood = 0 \\ \frac{Q_{b,t} - \bar{Q}_b}{\sigma_b} & : Flood = 1 \end{cases} \tag{3}$$

where $I_{b,t}$ is the intensity of the flood in basin b at date t, $Q_{b,t}$ is the stream flow in the same basin at the same time and $\bar{Q}_b$ and σ_b are mean and standard deviation of stream flow in b. The intensity is set to zero if the flood threshold - 95th percentile plus 1 standard deviation above the average - has not been exceeded. By normalizing, we obtain a measure that is comparable across all regions and that is independent of the absolute river flows. The assumption is that people living close to rivers will be prepared for variations in water levels, and that people living close to rivers with highly variable stream flows are more prepared for these events than people living close to more stable rivers.

To aggregate the flood impact each basin is weighted based on the nightlights in it. The weights per basin, $W_{b,t-1}$, used are:

$$W_{b,t-1} = \frac{L_{b,t-1}}{L_{p,t-1}} = \frac{\sum_i^I L_{i,t-1}}{\sum_j^J L_{j,t-1}} \tag{4}$$

where $L_{b,t-1}$ is the sum of lights in basin b one year, $t-1$, before the flood year and $L_{p,t-1}$ is the same at a province level.

Finally, the weights from (4) are multiplied with the intensity from (3) to get the overall flood impact, $FI_{b,t}$ in that basin on the province:

$$FI_{b,t} = W_{b,t-1} * I_{b,t} \tag{5}$$

One thing to note here is that for basins that span several provinces or districts, we have assumed the same intensity, but the weight is based on nightlights within each individual province.

4.1.2 Results

The stream flow was simulated for 5,082 consecutive days, from 1 February 2001 to 31 December 2014.[9] Table 2 shows that the top 10 basins with most flood days had close to 200 days of flooding over the 14-year period. As expected, these basins do overlap with some of the busiest flood areas according to the DFO, as shown in Figure 6. The lower part of Table 2 reveals that the driest basin had a mere 12 days of flooding. All 33 provinces with a basin had days that went above our flood threshold set in Equation (2).

All months in our model have flood events, but there are big differences. The range goes from 527 events every March and down to 154 events every August, with the traditional rainy season (November-March) producing the highest number of flood events, whereas the dry season months (June-October) are the driest. Aggregating the numbers for the rainy season, there are 2,215 events every year across the basins, while there are only 995 events every year during the dry season.

Total number of basins that are partly or fully inside Indonesia is 495, and these basins have a total of 55,605 flood events or slightly more than 112 per basin. In other words, the average basin has been flooded for a total of 8 days a year over the 14-year period in question. This is not entirely unexpected given the climate in Indonesia and the way our threshold is made. Also, if we compare with the DFO data where they have 3,808 floods of magnitude 4 or higher through their period from 1985-2016, which converts to almost 123 fairly large scale flood events per year, our model provides a reasonable proxy for events.

Even though the results seem logical on a per basin basis, the time steps in the model are 1 day at a time, which is too slow for the unfolding of a flood event, implying that downstream basins that would normally fill up very quickly will now only be filled up the day after, and then the next basin will be filled two days later and so forth. This means that the amount of days with floods are inflated. We believe that this does not affect our results much, though, as the number of events per province will not affect the end results, since we weigh by affected nightlight and not by number of days of floods.

Despite the numerous floods in Indonesia, they generally do not affect a large percentage of the population, as per Table 3. The mean of nightlights when excluding areas with 0 nightlight is 3.39 percent.

[9] For Bali we did it for 5,080 days due to problems with 30 and 31 December 2014.

Figure 6: Top 10 Most Flooded Basins and DFO Floods

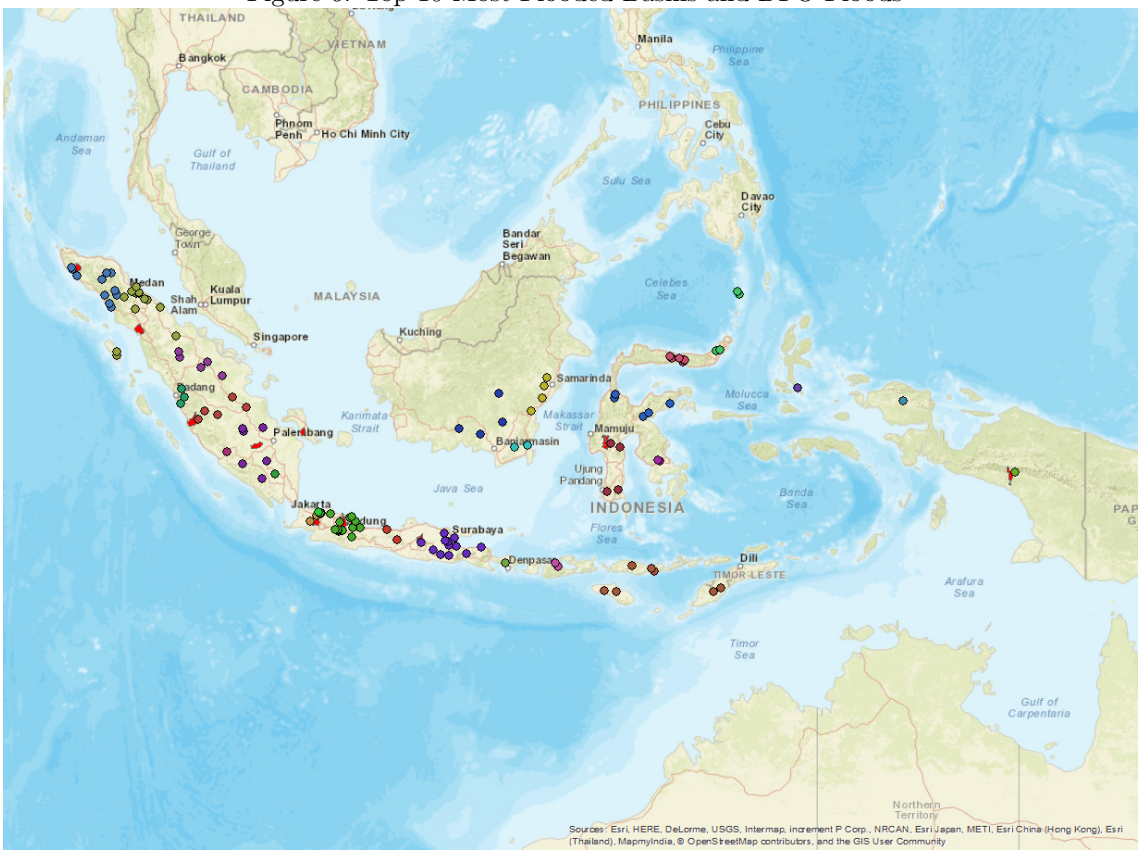

Table 2: Basins with Most and Least Flood Events

Basin Number	Affected Provinces	Number of flood events
2	Bangka-Belitung	192
705	Sumatera Selatan	190
133	Aceh	189
632	Jambi, Sumatera Barat	189
282	Sumatera Utara	187
872	Jawa Barat	186
868	Jawa Barat, Banten	183
916	Jawa Tengah, Jawa Timur	183
558	Sulawesi Barat, Sulawesi Selatan	180
709	Papua	177
256	Kalimantan Barat, Kalimantan Tengah	12
444	Riau	17
197	Sulawesi Tengah	21
316	Kalimantan Barat	24
314	Kalimantan Barat	27

If we assume that 3.39 percent of the approximately 250 million people of Indonesia are affected, the floods would impact 8.5 million people.

Table 3: Descriptives of Weights and Intensity (excluding zero damage observations)

Statistic	N	Mean	St. Dev.	Min	Max
Weights	45,005	0.034	0.060	0.00003	0.557
Intensity	45,005	4.516	2.608	0.989	50.944
Damage Index	45,005	0.155	0.351	0.0001	12.780

4.1.3 Comparison of Model versus DFO Floods

The DFO flood database is mostly based on news sources, providing an overview of the big floods in Indonesia. To check the database against the GeoSFM model, the focus will be on the largest events of magnitude 6 and above. Given how the DFO data do not give any intensity estimates and focus primarily on displacement numbers and area, while our model is driven by intensity the comparison will only focus on whether GeoSFM results do overlap in time and/or province with the centroid of the DFO floods.

Table 4 shows the DFO data on the left side, first column being the start month of the flood, followed by duration, magnitude, the province where the centroid of the flood is, dead and displaced. The right side shows the modeling results where the focus is on duration. The first column under model results shows the number of days for the centroid province, then overall number of days with floods anywhere in Indonesia during the period, then looking at the same island - using that as a proxy for neighboring regions - where one examines total days the island provinces were flooded during the flood and finally how many of the days of the flood duration that a province on the same island was flooded.

Generally, the model performs well, in particular on Sumatra and Kalimantan (Borneo), with the example where the 2008 flood was captured for all 25 days in the centroid province. Overall, it shows at least one flooded basin on Kalimantan and Sumatra for 85% of the days the major floods happened. The results are somewhat worse on Java, where only 37% of the days have a flood. A primary reason for this might be that Java is very narrow and hence the streams are short and might not be captured in our model. Java also has larger percentage of land not covered by a basin, ref Figure 5, also due to its narrowness which makes the low resolution landcover data underestimate the size of the basins.

4.1.4 Aggregated numbers

Finally, to aggregate up to a district or province level, we have used a simple method for the total damage experienced per year:

$$PD_{j,T} = \sum_{t}^{T} \sum_{b}^{B} FI_{j,b,t} \tag{6}$$

where j is the province or district, T is the year, sum of t is all the days for year T, sum of b are all the basins in the province or district and $FI_{b,t}$ is the flood impact from Equation 5. Normally one might use an average flood impact across the year, but by doing this, we capture repeated flood events and areas that experience generally high flooding.

Using the above method, Table 5 provides the aggregated data for all provinces across all years. The impact is fairly even for the most impacted ones, with the impact numbers for the top 10 ranging from 44 to 55. Furthermore, Sumatera Selatan, Lampung and Yogyakarta make up 8 of the top 10 impacted provinces. The overall picture fits with the DFO floods in Figure 1, with the populous provinces in Java, Sumatra and Sulawesi being impacted, whereas the smaller island provinces and parts of Kalimantan are not affected much. For some of the island provinces the numbers are probably underestimated, no basins will have been constructed and modeled there due to the many small islands.

Finally, Table 6 shows the most impacted districts over the years 2001 through 2014. The impact is much larger than for the provinces as one would expect due to the more localized data and impact. The districts are also more geographically spread out than the provinces.

Table 4: DFO Floods Compared with GeoSFM Results

	DFO Data					Model Results			
Date	Duration	Magnitude DFO	Centroid Province	Dead	Displaced	Flooded days in Province	Total Flood Days Sum All Provinces	Total Flood Days Sum on Island	Days Flooded on Island During Period
Jan 2002	17	6.1	Jawa Timur	147	380,000	5	17	8	7
Dec 2003	45	6.9	Jambi	148	350,000	18	45	180	41
Jan 2005	31	6.4	Sumatera Selatan	9	0	16	30	105	30
Jan 2006	20	6.2	Jawa Barat	19	10,000	6	20	13	9
May 2007	25	6.0	Kalimantan Tengah	0	3,000	23	25	79	25
Mar 2008	25	6.3	Riau	0	60,000	25	25	149	25
Apr 2010	17	6.2	Kalimantan Tengah	0	0	14	17	38	17
Feb 2012	8	6.2	Sumatera Selatan	0	1,200	6	8	27	8
Jan 2014	31	6.2	Jawa Barat	23	20,000	9	31	31	13

Table 5: Aggregated Flood Intensity Data by Province

Province	2001	2002	2003	2004	2005	2006	2007	2008	2009	2010	2011	2012	2013	2014
Aceh	12.674	7.400	14.712	11.213	18.127	15.643	23.155	20.799	17.918	20.076	17.665	10.116	14.864	10.571
Bali	3.614	11.780	13.083	11.676	10.359	10.783	8.080	5.786	9.042	7.851	7.882	7.609	8.580	
Bangka-Belitung	1.380	1.756	1.194	1.525	1.973	0.803	0.794	0.306	0.456	0.745	1.165	0.606	0.623	0.691
Banten	7.118	7.632	13.076	14.360	11.899	9.668	27.980	19.316	14.921	21.456	12.783	15.288	7.630	4.890
Bengkulu	6.394	6.756	25.205	13.606	14.273	10.266	11.683	16.207	13.145	17.983	17.417	6.351	21.045	7.279
Gorontalo	54.770	16.760	37.260	25.281	35.026	37.234	27.620	21.607	31.719	5.607	10.702	3.680	20.092	15.921
Irian Jaya Barat	1.368	0.647	1.242	0.565	1.167	0.921	0.985	0.508	1.107	0.356	0.343	1.837	1.710	1.307
Jakarta Raya	15.099	7.370	12.681	3.931	18.294	9.950	22.154	40.751	23.394	22.670	24.347	25.294	21.573	9.362
Jambi	44.338	11.141	10.589	11.677	19.131	13.241	16.989	34.894	31.627	32.430	15.023	21.463	32.401	30.362
Jawa Barat	16.616	17.697	29.439	18.629	30.536	23.842	36.484	28.958	27.030	35.907	25.600	27.714	29.462	11.156
Jawa Tengah	29.271	41.395	42.206	35.024	26.358	24.512	28.825	27.113	31.001	22.795	20.560	20.117	25.344	14.672
Jawa Timur	13.567	17.287	25.731	21.652	22.093	19.205	28.864	19.975	24.997	28.016	12.384	16.611	28.322	11.372
Kalimantan Barat	3.833	6.570	7.145	6.320	13.792	5.801	8.921	9.740	8.574	6.321	4.663	6.273	13.122	17.092
Kalimantan Selatan	26.550	10.917	19.599	21.410	15.397	12.302	21.088	29.202	21.391	16.995	10.598	29.563	32.648	21.549
Kalimantan Tengah	11.208	16.090	38.512	37.649	27.149	20.731	32.001	29.097	26.581	8.915	17.965	18.792	31.707	23.723
Kalimantan Timur	7.603	3.046	11.437	7.066	9.124	9.208	15.114	14.168	24.098	15.236	15.408	11.198	16.020	10.496
Kalimantan Utara	1.098	3.949	8.894	1.245	5.471	6.455	12.065	24.721	16.620	6.085	4.615	5.597	7.374	10.416
Lampung	25.228	20.499	30.012	32.566	31.452	21.910	23.642	37.172	39.414	49.285	25.333	22.493	43.979	47.995
Maluku	0.000	0.000	0.216	0.000	0.000	0.014	0.000	0.000	0.000	0.000	0.358	0.000	0.278	0.705
Maluku Utara	0.904	0.959	0.241	0.510	1.006	2.406	1.574	1.873	0.353	1.230	1.749	2.629	0.913	0.796
Nusa Tenggara Barat	0.014	0.083	0.035	0.021	0.080	0.034	0.059	0.093	0.036	0.038	0.064	0.068	0.048	0.009
Nusa Tenggara Timur	6.168	9.770	15.109	15.209	15.937	7.311	10.590	10.489	6.032	9.166	9.506	8.517	12.688	5.676
Papua	17.567	5.837	18.616	15.338	18.461	11.763	30.377	31.351	24.332	31.378	25.779	24.328	35.261	28.788
Riau	7.063	20.727	17.103	11.778	20.699	17.433	35.765	26.883	23.667	29.925	25.391	15.855	20.114	41.465
Sulawesi Barat	6.880	9.094	2.650	3.918	4.512	4.888	5.244	14.403	4.637	5.044	5.727	3.625	3.596	14.663
Sulawesi Selatan	14.729	9.733	14.866	12.397	8.112	15.667	11.431	14.619	12.996	9.001	10.157	7.805	11.202	12.707
Sulawesi Tengah	2.798	2.603	10.433	24.693	10.258	14.202	2.255	12.771	8.280	0.427	9.320	4.415	7.999	5.688
Sulawesi Tenggara	2.861	2.092	6.197	2.396	13.335	5.188	14.381	11.368	3.927	4.990	4.428	2.474	4.780	1.015
Sulawesi Utara	4.253	2.709	8.590	6.575	5.250	6.360	6.551	7.062	3.813	8.950	4.976	5.710	4.719	6.018
Sumatera Barat	8.944	16.785	26.946	21.787	28.464	18.737	35.011	24.624	24.595	18.317	9.770	10.559	17.472	18.169
Sumatera Selatan	27.938	17.191	47.852	33.865	34.345	23.193	39.282	55.345	34.210	34.032	24.159	23.462	51.858	27.107
Sumatera Utara	13.788	11.627	17.135	11.155	19.981	14.664	15.477	19.144	16.001	18.513	15.272	15.037	21.185	20.517
Yogyakarta	37.598	27.613	42.810	24.707	25.250	37.895	20.736	49.592	44.909	29.360	35.296	41.184	41.429	30.332

Table 6: 10 Most Impacted Districts

District	Province	Year	Flood Impact
Seruyan	Kalimantan Tengah	2010	175.080
Aceh Tengah	Aceh	2010	165.381
Bener Meriah	Aceh	2010	139.742
Pasaman	Sumatera Barat	2010	125.854
Sarolangun	Jambi	2010	118.244
Lubuk Linggau	Sumatera Selatan	2003	114.790
Keerom	Papua	2009	114.289
Tana Toraja	Sulawesi Selatan	2013	106.886
Klaten	Jawa Tengah	2002	106.488
Sukoharjo	Jawa Tengah	2002	106.488

5 Earthquake Damage Index

The measurement of earthquake detection and intensity has improved with remote sensing techniques. There are different methods to assess intensity and damage, ranging from satellite images (Dell'Acqua & Gamba, 2012; Tralli *et al.*, 2005; Gillespie *et al.*, 2007) to contour maps generated by seismological ground stations (De Groeve *et al.*, 2008; GeoHazards International and United Nations Centre for Regional Development, 2001; Federal Emergency Management Agency, 2006).

This paper uses the latter method, by utilizing ShakeMaps from USGS, which are automatically generated maps providing several key parameters following an earthquake, such as peak ground acceleration (PGA), peak ground velocity (PGV) and modified Mercalli intensity (MMI). More specifically, the ShakeMaps use data from seismic stations that is interpolated using an algorithm which is similar to kriging. To model the intensity in a given coordinate, the model also takes into account ground conditions and the depth of earthquake. Wald *et al.* (2005) point to the magnitude and epicenter location - which are parameters common for the entire earthquake - that have historically been used to determine how severe earthquakes were, but that the damage pattern is not just dependent on those two parameters, but also on other, more localized parameters that the ShakeMaps use to generate intensity measures.

This is exemplified by several earthquakes such as magnitude 6.7 and 6.9 earthquakes in California in 1994 and 1989, respectively, where some areas further away from the epicenters got more damaged than closer areas. The reason why the more localized ShakeMaps with their ground shaking parameters are a better gauge than magnitude and epicenter distance is explained on page 13 of Wald *et al.* (2005) which states that: "..., although an earthquake has one magnitude and one epicenter, it produces a range of ground shaking levels at sites throughout the region depending on distance from the earthquake, the rock and soil conditions at sites, and variations in the propagation of seismic waves from the earthquake due to complexities in the structure of the Earth's crust." The ShakeMaps are interpolated grids with point coordinates spaced approximately 1.5 kilometers apart (0.0167 degrees). Figure 2 shows contoured maps of these points.

The PGA is a measure of the maximum horizontal ground acceleration as a percentage of gravity, PGV is the maximum horizontal ground speed in centimeters per second and MMI is the perceived intensity of the earthquake, a subjective measure. Figure 7 - which is originally found in Wald *et al.* (1999) - explains the relationship between the different parameters and the potential damage from different values. The assumption is that damage starts at an MMI level of V and a PGA of 3.9 percent of g. These levels are found for California in Wald *et al.* (1999), but the relationship has been found for other areas in the US in Atkinson & Kaka (2006) and Atkinson & Kaka (2007) and for places such as Costa Rica (Linkimer, 2007) and Japan, Southern Europe and Western US (Murphy & O'Brien, 1977). It should be noted that the numerical relationship differs from region to region. There are no known papers estimating these values specifically for Indonesia.

Figure 7: ShakeMap Instrumental Intensity Scale Legend

PERCEIVED SHAKING	Not felt	Weak	Light	Moderate	Strong	Very strong	Severe	Violent	Extreme
POTENTIAL DAMAGE	none	none	none	Very light	Light	Moderate	Moderate/Heavy	Heavy	Very Heavy
PEAK ACC.(%g)	*<.17*	*.17-1.4*	*1.4-3.9*	*3.9-9.2*	*9.2-18*	18-34	34-65	65-124	>124
PEAK VEL.(cm/s)	<0.1	0.1-1.1	1.1-3.4	3.4-8.1	8.1-16	*16-31*	*31-60*	*60-116*	*>116*
INSTRUMENTAL INTENSITY	I	II-III	IV	V	VI	VII	VIII	IX	X+

Source: Wald *et al.* (1999)

The different measures are largely interchangeable, and in GeoHazards International and United Nations Centre for Regional Development (2001) report, they use PGA to measure damage, pointing to the fact that PGA, unlike MMI is an objective measure, implying that MMI is not easy to obtain reliably across the globe. Also, for large scale modeling, where it is unfeasible for one to model local conditions precisely, PGA serves as a good proxy for intensity of earthquakes.

5.1 Creation of Damage Index and Results

5.1.1 Damage Index

To construct the damage index, two types of data will be used; the intensity data - expressed as PGA - and building inventory data, to assess what damage one could expect for different intensities.

To take into account the building types in Indonesia, we use information from the USGS building inventory for earthquake assessment, which provides estimates of the proportions of building types observed by country; see Jaiswal & Wald (2008). The data provide the share of 99 different building types within a country separately for urban and rural areas. For Indonesia the building type information was compiled from a World Housing Encyclopedia survey, while the split between urban and rural is from the urban extent map of Center for International Earth Science Information Network - CIESIN - Columbia University *et al.* (2011). Without any other information available, we use this as an indication of the distribution of building types in Indonesia, but, necessarily, assume that the distribution is homogenous within urban and rural areas.

Fragility curves by building type are derived from the curves constructed by Global Earthquake Safety Initiative project; see GeoHazards International and United Nations Centre for Regional Development (2001). More specifically, buildings are first divided into 9 different types.[10] Each building type itself is then rated according to the quality of the design, the quality of construction, and the quality of materials. Total quality is measured on a scale of zero to seven, depending on the total accumulated points from all three categories. According to the type of building and the total points acquired through the quality classification, each building is then assigned one of nine vulnerability curves which provides estimates of the percentage of building damage for a set of 28 peak ground acceleration intervals.

In order to use these vulnerability curves for Indonesia we first allocated each of the 99 building types given in the USGS building inventory to one of the 9 more aggregate categories of the GESI building classification. However, to assign a building type its quality-specific vulnerability curve we would further need to determine its quality in terms of design, construction, and materials, an aspect for which we unfortunately have no further information. We instead assume that building quality is homogenous across building type in Indonesia and experiment with seven different sets of vulnerability curves, each set under a different quality ratings scenarios (ranging from 0 to 7).

Figure 8 depicts the building share weighted vulnerability curves of Indonesia for urban and rural areas.

Figure 8: Vulnerability Curves

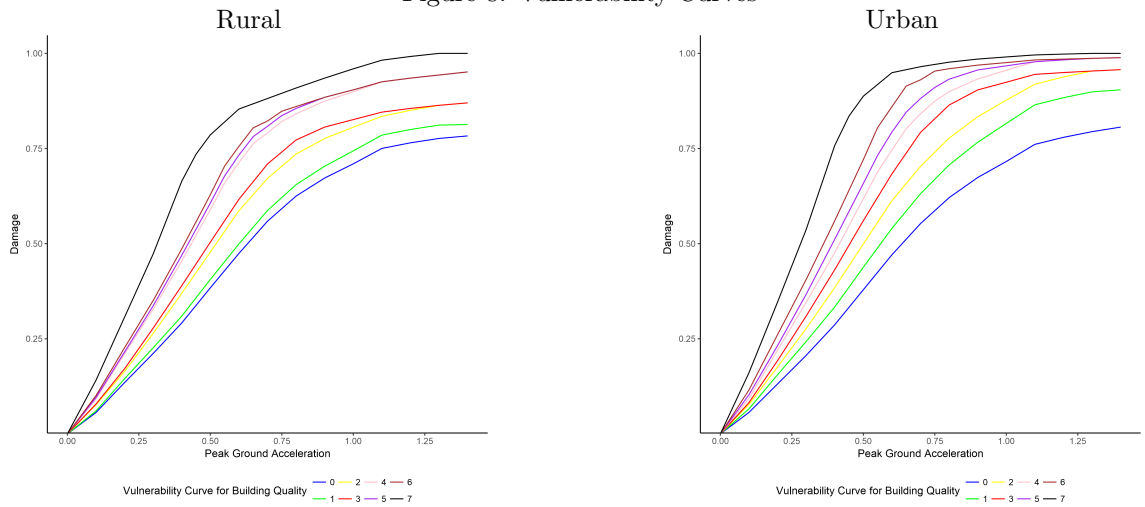

[10] Wood, steel, reinforced concrete, reinforced concrete or steel with unreinforced masonry infill walls, reinforced masonry, unreinforced masonry, adobe and adobe brick, stone rubble, and lightweight shack or lightweight traditional.

To model estimated damage due to a particular earthquake event the data from the ShakeMaps and GESI are used. Then, one identifies the value of peak ground acceleration that each nightlight cell in Indonesia experiences by matching each earthquake point with its nearest nightlight cell. If the cell is further away than 1.5 kilometers or if it experiences shaking (PGA) of less than 0.05 the value is set to 0. In order to derive at a region j specific earthquake damage index, ED, the following equation is applied:

$$ED_{q,j,t} = \sum_{i=1}^{I} w_{i,t-1} \sum_{k=1}^{K} \left(DR_{i,j,k,t}^{pga_{k,q}} \right) \qquad q = 0, \ldots, 7 \tag{7}$$

where DR is the damage ratio according to the peak ground acceleration, pga, and the urban-rural qualification of cell i, defined for a set of 8 different building quality q categories. The weight w_i is the same as before; the sum of the nightlights of the affected cells over the sum of the total provincial nightlights.

5.1.2 Results

With the above method, we find that 27 of the 34 provinces were damaged by earthquakes at some point in time.[11] Table 7 shows that the big islands Java and Sumatra have the most affected nightlight cells, given how densely populated they are and how much seismic activity is experienced there this is expected.

Table 7: Times a Lit Nightlight Cell is Damaged by Earthquake by Province

Province	Times Nightlight Cell Damaged	Percentage of Total
Aceh	1,170	22.28
Sumatera Utara	722	13.75
Sumatera Barat	511	9.73
Sulawesi Tengah	354	6.74
Jawa Barat	353	6.72
Sumatera Selatan	283	5.39
Jawa Tengah	259	4.93
Jawa Timur	242	4.61
Bengkulu	165	3.14

Finally, there were 5,251 cases where the instance hit a nightlight cell that was lit. Table 8 shows that the individual nightlight cell weights are small, as expected, but the impact of having buildings of quality 4 is that within a cell that is hit, on average a bit more than 6 percent of the buildings are destroyed.[12]

Table 8: Descriptives of Weights and Intensity for Building Quality 4 (excluding weights of zero)

Statistic	N	Mean	St. Dev.	Min	Max
Weights	5,251	0.226	0.407	0.009	9.328
Damage	5,251	0.062	0.043	0.046	0.547
Intensity	5,251	0.016	0.035	0.0004	0.859

Weights and Intensity multiplied by 1,000

[11] The seven not affected were Bangka Belitung, Kalimantan Barat, Kalimantan Selatan, Kalimantan Tengah, Kalimantan Timur, Kalimantan Utara and Kepualauan Riau.

[12] We did the same for buildings of quality 0 (the best) and 7 (the worst), something which led to maximum damage values of 33% for the best buildings and 84% for the worst versus 55% for our base case, showing how the overall damage is highly dependent on building quality information.

5.1.3 Aggregated data

When aggregating, a similar method as in section 4 is used, but now the aggregation is done directly by nightlight cells instead of by basin. The equation is:

$$ED_{j,t} = \sum_{l}^{L} ED_{l,t} \tag{8}$$

where t is year, l is all nightlight cells in the province or district j and ED is the damage from equation 7.

Table 9 provides the full overview of damage by province, showing the large differences between the provinces and how they vary from year to year, as one can expect with highly randomized events such as earthquakes. Using Yogyakarta - which was only impacted by earthquakes in 2006 - as an example, there was a loss of 0.4 percent of the total building mass, causing damages estimated to be approximately 3.1 billion US dollars in addition to more than 5,000 deaths and tens of thousands of injured and displaced people. Apart from that, provinces on Sumatra make up 6 of the top 10 most damaging years. Even though Indonesia is often hit by severe earthquakes, even in the worst of years they only destroy about 1 percent of the buildings in a province. That being said, 1 percent of total building mass and infrastructure being damaged does constitute a significant portion of local budgets. As another example, the September 2009 earthquake in West Sumatra inflicted damages for an estimated 2.3 billion US dollars, with repair costs and losses of 64 million US dollars on government buildings (Raschky, 2013).

The numbers per district are shown in Table 10, and they suffer much more damage than the provinces, with the most impacted district losing 5 percent of building mass.

Table 9: Aggregated Earthquake Damage Data by Province

Province	2004	2005	2006	2007	2008	2009	2010	2011	2012	2013	2014
Aceh	0.040	0.728	0.160	0.152	0.044	0.010	0.269	0.345	4.597	3.869	0.000
Bali	0.557					0.014		0.184			
Banten		0.003	0.268			0.032			0.142	0.022	
Bengkulu	0.447	0.623		8.905	0.380	0.270	0.378	0.154	1.224	0.176	
Gorontalo			0.021		0.929	0.000			0.404	0.000	
Irian Jaya Barat	0.030				0.178	0.410	0.000		0.000		1.217
Jakarta Raya						0.060					
Jambi				1.071	0.033	0.070	0.000				
Jawa Barat			0.018	0.047		0.171	0.007		0.047	0.000	
Jawa Tengah			0.404								
Jawa Timur			0.012							0.190	
Lampung			0.019	0.040		0.000					
Maluku	0.000	0.253	0.378	0.176	0.000	0.000	0.049		5.202	0.105	
Maluku Utara			0.095	0.769	0.644	0.000	0.000	0.147	0.238	4.216	0.918
Nusa Tenggara Barat		0.006	0.248	0.771	0.038	0.187	0.031				
Nusa Tenggara Timur	0.215	0.000		0.048	0.070	0.274		0.026	0.804		1.056
Papua	1.070		0.000	0.000	0.056	0.021	0.235	0.272	0.687	0.392	0.048
Riau		0.003		0.056		0.360					
Sulawesi Barat		0.000				0.123		1.431			
Sulawesi Selatan								0.261	0.000		
Sulawesi Tengah	0.000	0.654	0.185		0.180	0.659	0.050	1.513	5.346	0.000	
Sulawesi Tenggara		0.110	0.052		0.060			0.464			
Sulawesi Utara		0.069	0.050	0.651	0.011	0.263					0.111
Sumatera Barat	0.032	0.175	0.000	9.094	0.173	3.072	0.008	0.000	0.000	0.316	
Sumatera Selatan		0.000		0.816	0.000						
Sumatera Utara	0.002	0.208	0.072	0.010	0.041	0.022	0.175	2.175	0.048		0.000
Yogyakarta			4.318								

Note: Multiplied by 1,000

Table 10: 10 Most Impacted Districts

District	Province	Year	Intensity
Alor	Nusa Tenggara Timur	2014	53.184
Waropen	Papua	2010	45.070
Mukomuko	Bengkulu	2007	44.215
Aceh Tengah	Aceh	2013	41.736
Nabire	Papua	2004	39.864
Bener Meriah	Aceh	2013	37.750
Sangihe Talaud	Sulawesi Utara	2009	32.947
Lembata	Nusa Tenggara Timur	2012	31.692
Halmahera Selatan	Maluku Utara	2013	31.511
Aceh Barat	Aceh	2012	22.141

Note: Multiplied by 1,000

6 Volcano Damage Index

A volcanic eruption consists of ash clouds, pyroclastic flows and lava flows, the latter two which are very difficult to model without extensive local data. Unfortunately, there is little to no academic research that has looked into large scale volcanic modeling for all aspects of eruptions. For modeling ash clouds, Joyce *et al.* (2009) points to remote sensing through satellite images that detect SO_2 emissions as a potential method.

To construct a damage index for eruptions, we use a two-fold process. First, volcanic ash advisory data are used from Volcanic Ash Advisory Centers (VAAC) to detect eruptions; second, satellite images containing sulphur dioxide data from the OMI/AURA satellite are used to model the intensity of the eruptions. The OMI/AURA images have been utilized by Carn *et al.* (2009) and Ferguson *et al.* (2010) to model eruption intensity.

6.1 Volcano Modeling

There are at least two types of software that are used to model eruptions. Voris (Felpeto *et al.*, 2007), which models ash clouds, lava flows and energy cones, and HYSPLIT from Air Resources Laboratory, which models air pollution dispersion. Voris relies on highly localized data due to the lava flow and energy cone modeling, which one will not have in most cases and that does not fit well for large scale modeling across time and space. HYSPLIT does have batch inputs, but still requires several inputs per eruption, some which are not easily obtainable.

The third solution, which is related to the ash clouds mentioned by Joyce *et al.* (2009), is based off ash advisory data to determine whether an eruption happened and OMI/AURA satellite data to determine the scale of the eruption. This will not help with modeling lava flows and energy cones, but due to the very localized nature of the flows, there are no good sources or methods to model it for several eruptions from different volcanoes, leaving the ash clouds as a good proxy for all damages.

6.1.1 Ash advisory data

Ash advisories from the Darwin VAAC (DVAAC), which are ash cloud warnings for airplanes, are used to determine whether an eruption is happening. The warnings show relevant data such as volcano name, position, summit height, height of clouds and a color code that reflects the condition of the air/volcano. There are 4 different codes ranking from the normal state, green, to imminent danger of or ongoing volcanic eruption, red. Over the period from 2004 until 2015, the DVAAC issued 12,962 warnings and of these more than 90 percent were either of code red or orange. Data on advisories from code orange or below were not used, due to eruptions of this scale not being large enough to be properly captured by the SO_2-data. By limiting the data to code red events, there are 1,785 events spread across 587 dates.[13]

6.1.2 OMI/AURA Satellite images

To measure the intensity of an eruption, data from the Sulphur Dioxide images of the OMI/Aura project (Krotkov & Li, 2006) are used. These consist of satellite images from October 2004 and onwards. The data have been used to model ash cloud intensity and movement in several articles such as Carn *et al.* (2009) and Ferguson *et al.* (2010).

The satellite images have a spatial resolution of $13 * 24$km and are taken from 80km above ground. The spectral imaging shows the SO_2 vertical column density in Dobson Units and there are 14 or 15 orbits per day, where one orbit covers an area approximately 2,600km wide. A dobson unit is a measure of density, and at sea level the typical concentration in clean air is less than 0.2DU. The images contain 4 values for column density based on the center of mass altitude (CMA), which is a measure of the altitude one assumes the center of the distribution is at. There are 4 different estimates for the vertical column density, ranging from 0.9km above ground to 18km above ground.

[13] There were 571 different dates, but some of these dates issued red warnings to 2 or more volcanoes.

For volcanic activities one normally uses a CMA of either 8km or 18km (OMI team, 2012), where the former is a middle tropospheric column (TRM) and is for use in medium eruptions, while the latter is an upper tropospheric and stratospheric column (STL) and is for explosive eruptions. Despite this difference, the data are interchangeable in the sense that one can interpolate from one CMA to the others.

OMI is more sensitive above clouds, which both measures mentioned will normally be. The standard deviation for both measures is as low as 0.1DU over Indonesia. The data for both STL and TRM are very similar and this paper uses the STL-data as that are most useful for the biggest events.

6.2 Creation of Damage Index and Results

6.2.1 Damage Index

When constructing a damage index based on SO_2 values from ash clouds, one has to set thresholds for distance from the event and from the centroid of the nightlight cell and also a lower sulphur dioxide-value. There are no papers or literature that have estimated any parameter values and there are no usable local data, so the thresholds have been set somewhat arbitrarily.

First off, one wants to set a distance threshold estimating how far away the eruption could cause damage. Note that one wants ground results and not for the aviation industry, since planes can be affected very far away as evidenced by the total stand still of planes across Europe during the 2010 Eyjafjallajökull eruption. We decided to set a very relaxed condition with any point closer than 10 degrees of latitude and longitude included. Figure 9 portrays the plume approximately 7 hours after one of the biggest Merapi eruptions on 4 November 2010, where the plume moved relatively slowly and after 1000km it dissipated at the lower altitudes, which shows that our 10 degree threshold works well.

Secondly, to match the nightlight data with the OMI/Aura data, a maximum distance between a nightlight point and the nearest SO_2 point is set at 50km. The SO_2 points are fairly scattered due to cloud covers, hence to get a more consistent grid of nightlight and SO_2 values we have chosen a distance that is approximately two times the longest side of an OMI cell.

Finally, a minimum SO_2 value in Dobson Units is chosen. According to the Belgian Institute for Space Aeronomy, a typical normal level in air is 0.1DU and a strong eruption is above 10, which is the threshold value chosen.

Once the thresholds have been set, the same nightlight weighting method as for our other indices is applied and then the weights are multiplied with the SO_2 value to get an intensity value. The equation is:

$$VD_{i,t} = \begin{cases} 0 & : VSO2 < 10 \\ w_{i,T-1} * VSO2_i & : VSO2 \geq 10 \end{cases} \tag{9}$$

where i is the nightlight cell on date t, and $w_{i,T-1}$ is the previously used weight where i is the nightlight cell, $T-1$ is the nightlight strength from the prior year and it is divided by the sum of total nightlights in the province or district.

Figure 9: Merapi Ash-Cloud 4 November 2010 at 05.33UTC (7h post-eruption)

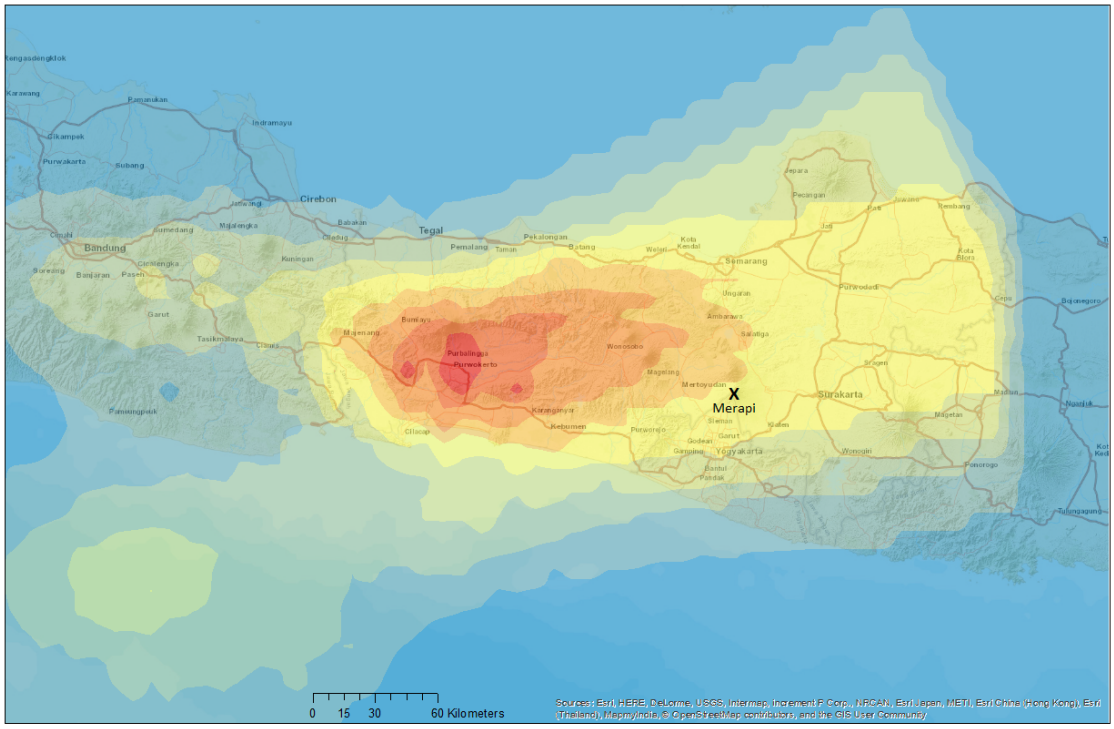

6.2.2 Results

Applying our constraints, the 587 dates with a red warning have been reduced to 16 days. Of these, 7 are from the 2010 eruption on Merapi, the biggest event during the time period.

Table 11 provides the affected nightlight cells by year and volcano and the results are closely correlated with the events of the period. The main one is the Merapi eruption in 2010, Soputan with volcanic explosivity index events of level 2 and 3 in 2004, 2005, 2007 and 2008 (Global Volcanism Program, 2013) and Sinabung with several eruptions in 2014, which all fit the model well.

Table 11: Nightlight Cells by Year and Volcano

Volcano	2004	2005	2007	2008	2010	2014	Total
Kelut						2,311	2,311
Manam		62					62
Merapi					129,352		129,352
Sangeang Api						1,156	1,156
Sinabung						3,566	3,566
Soputan	6,164	586	4,672	3,704			15,126
Total	6,164	648	4,672	3,704	129,352	7,033	151,573

Table 12 refer to province impacts, and the eruptions affected numerous provinces on Java and Sumatra, with Jawa Barat and Jawa Tengah being the most affected with more than 120,000 cells with an SO_2-value above 10 at some point. This is further underlined by nine of the ten most affected districts in Table 13 being in these two provinces, which are linked to the Merapi eruption in 2010. Apart from that, Sulawesi Utara were affected all the years from 2004 through 2008 by the eruptions on Soputan.

The final table in this section, Table 14, provide descriptives of the SO_2 variable and the nightlight weights, as well as the product of the two. Overall, the mean SO_2 value during these events is almost 20, with a max close to 60, which is 600 times the normal level of 0.1DU SO_2.

Table 12: Affected Nightlight Cells by Province and Year

Province	2004	2005	2007	2008	2010	2014	Total
Aceh						2,078	2,078
Banten					940		940
Jawa Barat					52,034		52,034
Jawa Tengah					71,356		71,356
Jawa Timur					2,320	2,311	4,631
Nusa Tenggara Timur						1,156	1,156
Papua		62					62
Sulawesi Utara	6,164	586	4,672	3,704			15,126
Sumatera Utara						1,488	1,488
Yogyakarta					2,702		2,702
Total	6,164	648	4,672	3,704	129,352	7,033	151,573

Table 13: Top 10 Districts with Most Affected Nightlight Cells

District	Province	Affected Cells
Cilacap	Jawa Tengah	16,114
Sukabumi	Jawa Barat	10,724
Kebumen	Jawa Tengah	10,080
Ciamis	Jawa Barat	9,612
Banyumas	Jawa Tengah	9,384
Cianjur	Jawa Barat	8,260
Brebes	Jawa Tengah	6,112
Minahasa Selatan	Sulawesi Utara	5,960
Garut	Jawa Barat	5,622
Bandung	Jawa Barat	5,342

Table 14: Descriptives of Weights and Intensity (Excluding weights of zero)

Statistic	N	Mean	St. Dev.	Min	Max
Weights	114,587	0.046	0.084	0.007	2.354
SO2 level	114,587	19.748	10.556	10.083	57.231
Intensity	114,587	0.855	1.707	0.075	42.857

Weights and Intensity multiplied by 1,000

6.2.3 Aggregated data

To aggregate the data, the same method as before is applied, with:

$$VD_{j,T} = \sum_{t}^{T} \sum_{i}^{I} VD_{i,t} \tag{10}$$

where all days t of year T and all nightlight cells i in province or district j are aggregated.

The province overview, shown in Table 16, is caused by the Merapi eruption, with 3 of the top 4 being due to that eruption. Jawa Tengah and Yogyakarta are the two most affected provinces, given their immediate proximity to Merapi. One thing to note is that Jawa Timur, which is east of Merapi, was hardly affected at all.

For districts, the Merapi results are even more pronounced, with all districts in the top 10 being from the 2010 eruption. All the Jawa Tengah districts are west of the volcano. It is somewhat surprising to find that some of the districts in the immediate vicinity of Merapi are not on the list, but this can be due to the timing and quality of the satellite images. Given the time interval between images, the SO_2

clouds could have traveled past the closest districts by the time an image was taken. Regardless, the results are uniform in that all affected districts are neighbors. Overall, the model seems to give a fair picture of when and where the eruptions were at their most intense, although the ground level intensity can be hard to specify.

Table 15: 10 Most Impacted Provinces

Province	Year	Intensity
Jawa Tengah	2010	34.641
Yogyakarta	2010	18.607
Sulawesi Utara	2004	16.224
Jawa Barat	2010	10.271
Sulawesi Utara	2007	6.387
Sulawesi Utara	2008	4.861
Nusa Tenggara Timur	2014	2.356
Aceh	2014	2.134
Sulawesi Utara	2005	0.684
Jawa Timur	2010	0.660

Note: Multiplied by 1,000

Table 16: Aggregated Volcano Intensity Data by Province and Year

Province	2004	2005	2007	2008	2010	2014
Aceh						2.134
Banten					0.163	
Jawa Barat					10.271	
Jawa Tengah					34.641	
Jawa Timur					0.660	0.432
Nusa Tenggara Timur						2.356
Papua		0.061				
Sulawesi Utara	16.224	0.684	6.387	4.861		
Sumatera Utara						0.487
Yogyakarta					18.607	

Table 17: 10 Most Impacted Districts

District	Province	Year	Intensity
Purwokerto	Jawa Tengah	2010	184.673
Banyumas	Jawa Tengah	2010	168.916
Cilacap	Jawa Tengah	2010	149.878
Kebumen	Jawa Tengah	2010	141.635
Banjarnegara	Jawa Tengah	2010	106.472
Purbalingga	Jawa Tengah	2010	98.697
Purworejo	Jawa Tengah	2010	92.593
Kulon Progo	Yogyakarta	2010	72.177
Wonosobo	Jawa Tengah	2010	69.568
Banjar	Jawa Barat	2010	60.208

Note: Multiplied by 1,000

7 Tsunami Damage Index

The final disaster damage index constructed is for the 2004 Christmas tsunami. There is little local district level damage data available, so it was decided to use the methodology from Heger (2016), whereby inundation maps are used to construct a district level damage index assuming a uniform damage across all flooded areas.

7.1 Creation of Damage Index and Results

7.1.1 Damage Index

Despite all the media coverage and attention the 2004 tsunami had, there is not much detailed spatial information readily available for research. Heger (2016) has done some research on the causal effects of the tsunami in his PhD thesis, and we will follow his method closely to model flood impact.

To construct an inundation map of the affected areas, a map based on MODIS satellite pictures from Anderson *et al.* (2004) is used. The map itself is fairly low resolution, but it provides a good overview of the inundated areas. In terms of the intensity of the flood, there are no existing data on that, but a uniform flood intensity across all flooded areas is assumed, just as in Heger (2016). The resulting map is shown in Figure 10, which shows that a large proportion of the Aceh coastline was struck by the tsunami.

To make this map, the inundation map from DFO was used as a base. Spatial algorithms were then applied to detect the difference in color between inundated and non-inundated areas. This process started with overlaying the base map on a regular shapefile of Indonesia, then detecting the specific color of inundated areas, before constructing a new shapefile where all inundated areas (areas with the same color) have value 1 and all other areas have value 0.

Figure 10: Inundation Map of 2004 Tsunami

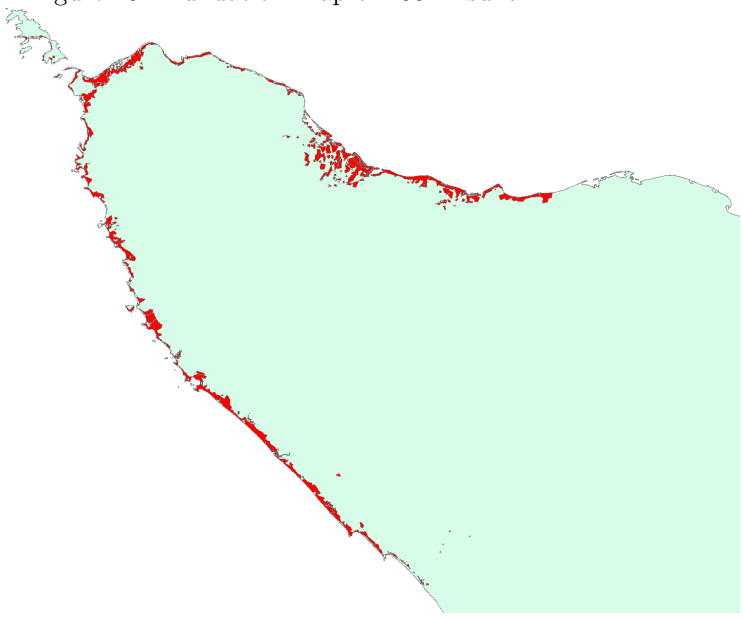

7.1.2 Results

Figure 11 shows the inundated area nightlight cells, combined with the nightlight cells in all of Aceh. The tsunami did not strike the most densely populated areas, 460 nightlight cells were hit, out of a total of 13,456 cells in all of Aceh. Given that the tsunami happened 26 December 2004, it is more appropriate to link the incident with the 2004 nighlights, instead of 2003, as is done for the other disaster types. Using the 2004 numbers, there were 364 lit inundated cells out of 7,607 total lit cells in Aceh. Interestingly, in 2005, the year after the disaster, there is a strong decline, with 306 and 6,352 lit cells for the inundated

areas and Aceh, respectively. The average light intensity has gone down, from 7.39 per cell to 6.33 in the inundated areas and from 6.37 to 5.18 in the province as a whole.

Figure 11: Aceh Nightlights and Tsunami Affected Nightlights

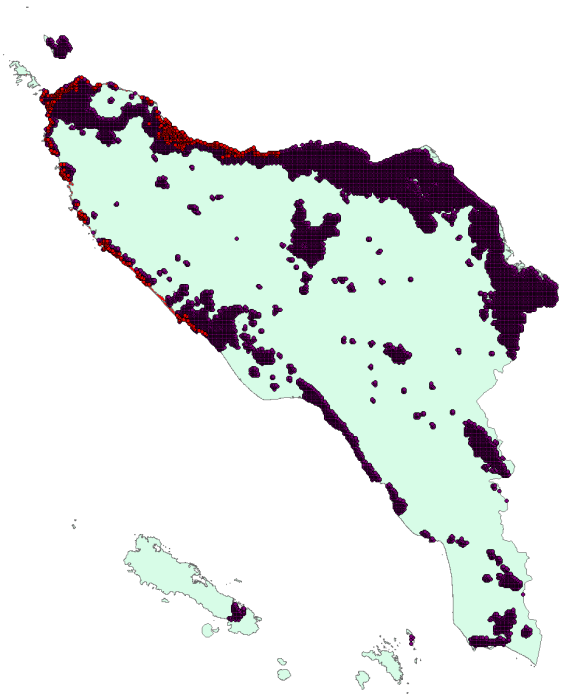

Finally, Table 18 shows the weights which are - again - defined as nightlight in the cell over total nightlight in the province. Although the numbers look very small, by multiplying the means by number of cells, one gets approximately 5.5 percent. Knowing that the census numbers for Aceh in 2000 gave a population of just under 4 million and in 2010 of just under 4.5 million and if one multiplies the population numbers with the affected cells number of 5.5 percent of the total, one gets 221,894 and 249,631, respectively. Given the official numbers of 166,671 dead due to the tsunami, an assumption of total destruction in all inundated areas seem a bit high, given that 166,671 of 230,000 is 72.47 percent. A damage of 75 percent in the inundated cells is chosen, giving a final damage index formula:

$$TD_i = W_i * D \tag{11}$$

where TD_i is the province weighted damage from nightlight cell i, $W_i = \frac{l_i}{\sum_i^I l_i}$ i.e. the light in cell i over the sum of all nightlight in the province and D is the flat damage number of 0.75.

Table 18: Descriptives of Weights by Year

	All Cells		Only Lit Cells	
Year	Cells	Mean[a] (st.dev[a])	Total Cells	Mean[a] (st.dev[a])
2003	460	0.0965 (0.1356)	295	0.1505 (0.1433)
2004	460	0.1206 (0.1369)	364	0.1524 (0.1373)
2005	460	0.1281 (0.1656)	306	0.1925 (0.1698)

a. Multiplied by 1000

7.1.3 Aggregated data

Aggregating the data is done using the same method as in all previous sections, where the nightlight cells across the province or district is summed up:

$$TD_j = \sum_{i}^{I} TD_i \tag{12}$$

where all nightlight cells i in province or district j are aggregated.

Since the tsunami only affected one province, it is easy to see the total damage done by it on Aceh. With our assumptions, the tsunami destroyed about 4 percent of the buildings in Aceh. This is clearer once broken down into district level damage. There were 6 districts affected by the tsunami, with Aceh Jaya, Banda Aceh and Pidie all experiencing damage of more than 20 percent. The other 3 affected districts - Aceh Barat, Aceh Besar and Bireuen - experienced damage between 5 and 10 percent due to the tsunami.

Table 19: Aggregated Tsunami Damage by District and Province

District	Province	Intensity
Aceh Barat	Aceh	0.071
Aceh Besar	Aceh	0.078
Aceh Jaya	Aceh	0.221
Banda Aceh	Aceh	0.229
Bireuen	Aceh	0.055
Pidie	Aceh	0.210
Aggregated	Aceh	0.042

8 Conclusion

With the continuous increase in remote sourcing data, it has gotten much easier and cheaper to monitor and assess the damages from natural disasters. Joyce *et al.* (2009) and Gillespie *et al.* (2007) have done an extensive review of how satellite images can be used to map natural disasters, while this paper has contributed with providing new techniques that utilize other remote sourced data such as ShakeMaps and ash advisory data.

Throughout, techniques based on freely available data have been used to construct damage indices for different disaster types. Generally the indices can be used in any area of the world, and if calibrated with local data, they could provide an excellent tool for local governments or stakeholders in early disaster assessments.

The indices can be used to get quick damage estimates and inform where to provide relief, as well as in research such as what the authors have done in Skoufias *et al.* (2017), where the indices are used to analyze district budget redistributions following natural disasters.

The main caveat is the indices have not been validated against local level damage data. If one had access to high resolution monetary or intensity data, the estimates would be much more precise.

Table 20 gives an overview of the different data sources and software used. All disasters have used the DMSP global nightlights data to weight the indices based on economic activity. Recently, the VIIRS nightlight data provide an alternative for assessing economic activity or events, as showcased for GDP in China (Li *et al.*, 2013; Shi *et al.*, 2014) and Africa (Chen & Nordhaus, 2015) and for storms and floods in the US (Cao *et al.*, 2013; Sun *et al.*, 2015). If one is interested in events after 2012, the VIIRS data provide higher spatial resolution and track changes by month instead of yearly.

Alternatives do exist for choice of software if one wants everything to be open source and free. Instead of ArcGIS, packages such as QGIS and RGDAL for R are potential alternatives. R and Python are used more and more for spatial data and can often provide the necessary tools to do the modeling. Instead of statistical software such as Matlab and Stata, R and Python once more provide excellent alternatives.

Table 20: Disasters and the Data Sources and Softwares used

Disaster Type	Data Sources	Software Used
Flood	Hydro1K GLCC FAO Digital Soil Map TRMM GDAS	GeoSFM (ArcView 3.3) Python Stata ArcGIS
Earthquake	USGS ShakeMaps USGS Building Inventory World Housing Encyclopedia Urban Extent Map (CIESIN) GESI	Python Stata ArcGIS
Volcanic Eruption	Ash Advisory Data OMI/AURA Satellite Images	Python Matlab Stata ArcGIS
Tsunami	DFO Inundation Map	Python ArcGIS Stata

References

Anderson, Elaine, Brakenridge, G.R., & Caquard, Sébastien. 2004. *DFO Event number 2004 - 193 - Aceh Province Inundation Map 1.* http://www.dartmouth.edu/ floods/2004193.html. Online; accessed 1 June 2016.

Artan, G.A., Asante, K., Smith, J., Pervez, S., Entenmann, D., Verdin, J., & Rowland, J. 2008. *Users Manual for the Geospatial Stream Flow Model (GeoSFM): U.S. Geological Survey Open-File Report 20071440.* User Manual. USGS.

Asante, Kwabena O., Macuacua, Rodrigues D., Artan, Guleid A., Lietzow, Ronald W., & Verdin, James P. 2007. Developing a Flood Monitoring System From Remotely Sensed Data for the Limpopo Basin. *IEEE Transactions on Geoscience and Remote Sensing*, **45**(6), 1709–1714.

Athukorala, Prema-chandra, & Resosudarmo, Budy P. 2005. The Indian Ocean Tsunami: Economic Impact, Disaster Management, and Lessons. *MIT Press*, **4**(1), 1–39.

Atkinson, Gail M., & Kaka, SanLinn I. 2007. Relationships between Felt Intensity and Instrumental Ground Motion in the Central United States and California. *Bulletin of the Seismological Society of America*, **97**(2), 497–510.

Atkinson, Gail Marie, & Kaka, SanLinn I. 2006. *Relationships between felt intensity and instrumental ground motion for New Madrid ShakeMaps.* Department of Earth Sciences, Carleton University.

Balk, D.L., Deichmann, U., Yetman, G., Pozzi, F., Hay, S.I., & Nelson, A. 2006. Determining Global Population Distribution: Methods, Applications and Data. *Pages 119–156 of: Advances in Parasitology.* Elsevier.

Brakenridge, R., & Anderson, E. 2006. MODIS-based flood detection, mapping and measurement: The potential for operational hydrological applications. *Pages 1–12 of:* Marsalek, Jiri, Stancalie, Gheorghe, & Balint, Gabor (eds), *Nato Science Series: IV: Earth and Environmental Sciences.* Springer Netherlands.

Cao, Changyong, Shao, Xi, & Uprety, Sirish. 2013. Detecting Light Outages After Severe Storms Using the S-NPP/VIIRS Day/Night Band Radiances. *IEEE Geoscience and Remote Sensing Letters*, **10**(6), 1582–1586.

Carn, Simon A., Krueger, Arlin J., Krotkov, Nickolay A., Yang, Kai, & Evans, Keith. 2009. Tracking volcanic sulfur dioxide clouds for aviation hazard mitigation. *Natural Hazards*, **51**(2), 325–343.

Center for International Earth Science Information Network - CIESIN - Columbia University, International Food Policy Research Institute - IFPRI, The World Bank, & Centro Internacional de Agricultura Tropical - CIAT. 2011. Global Rural-Urban Mapping Project, Version 1 (GRUMPv1): Urban Extents Grid. Palisades, NY: NASA Socioeconomic Data and Applications Center (SEDAC). http://dx.doi.org/10.7927/H4GH9FVG. Accessed 02 01 2017.

Chen, Xi, & Nordhaus, William. 2015. A Test of the New VIIRS Lights Data Set: Population and Economic Output in Africa. *Remote Sensing*, **7**(4), 4937–4947.

Chung, Hsiao-Wei, Liu, Cheng-Chien, Cheng, I-Fan, Lee, Yun-Ruei, & Shieh, Ming-Chang. 2015. Rapid Response to a Typhoon-Induced Flood with an SAR-Derived Map of Inundated Areas: Case Study and Validation. *Remote Sensing*, **7**(9), 11954–11973.

De Groeve, Tom, Annunziato, A, Gadenz, S, Vernaccini, L, Erberik, A, & Yilmaz, T. 2008. Real-time impact estimation of large earthquakes using USGS Shakemaps. *Proceedings of IDRC2008, Davos, Switzerland.*

Dell'Acqua, Fabio, & Gamba, Paolo. 2012. Remote Sensing and Earthquake Damage Assessment: Experiences, Limits, and Perspectives. *Proceedings of the IEEE*, **100**(10), 2876–2890.

Dessu, Shimelis Behailu, Seid, Abdulkarim Hussein, Abiy, Anteneh Z., & Melesse, Assefa M. 2016. *Flood Forecasting and Stream Flow Simulation of the Upper Awash River Basin, Ethiopia Using Geospatial Stream Flow Model (GeoSFM).* Cham: Springer International Publishing. Pages 367–384.

Elvidge, Christopher, Baugh, Kimberly, Hobson, Vinita, Kihn, Eric, Kroehl, Herbert, Davis, Ethan, & Cocero, David. 1997. Satellite inventory of human settlements using nocturnal radiation emissions: A contribution for the global toolchest. *Global Change Biology*, **3**(5), 387–395.

Federal Emergency Management Agency. 2006. *HAZUS-MH MR2 Technical Manual.* Federal Emergency Management Agency, Washington, D.C.

Felpeto, Alicia, Mart, Joan, & Ortiz, Ramon. 2007. Automatic GIS-based system for volcanic hazard assessment. *Journal of Volcanology and Geothermal Research*, **166**(2), 106 – 116.

Ferguson, David J., Barnie, Talfan D., Pyle, David M., Oppenheimer, Clive, Yirgu, Gezahegn, Lewi, Elias, Kidane, Tesfaye, Carn, Simon, & Hamling, Ian. 2010. Recent rift-related volcanism in Afar, Ethiopia. *Earth and Planetary Science Letters*, **292**(34), 409 – 418.

Fu, Bihong, Awata, Yasuo, Du, Jianguo, Ninomiya, Yoshiki, & He, Wengui. 2005. Complex geometry and segmentation of the surface rupture associated with the 14 November 2001 great Kunlun earthquake, northern Tibet, China. *Tectonophysics*, **407**(1-2), 43–63.

GeoHazards International and United Nations Centre for Regional Development. 2001. *Final report: Global Earthquake Safety Initiative (GESI) pilot project.* Report. GHI.

Gillespie, T. W., Chu, J., Frankenberg, E., & Thomas, D. 2007. Assessment and prediction of natural hazards from satellite imagery. *Progress in Physical Geography*, **31**(5), 459–470.

Global Volcanism Program. 2013. *Volcanoes of the World, v. 4.5.3. Venzke, E (ed.). Smithsonian Institution. Downloaded 25 Jan 2017.*

G.R.Brakenridge. 2016. *Global Active Archive of Large Flood Events, Dartmouth Flood Observatory, University of Colorado.* http://floodobservatory.colorado.edu/Archives/index.html. Online; accessed 29 May 2016.

Haq, Mateeul, Akhtar, Memon, Muhammad, Sher, Paras, Siddiqi, & Rahmatullah, Jillani. 2012. Techniques of Remote Sensing and GIS for flood monitoring and damage assessment: A case study of Sindh province, Pakistan. *The Egyptian Journal of Remote Sensing and Space Science*, **15**(2), 135–141.

Heger, Martin Philipp. 2016. *The Causal Effects of the Indian Ocean Tsunami and Armed Conflict on Acehs Economic Development.* Ph.D. thesis, London School of Economics.

Henderson, J. Vernon, Storeygard, Adam, & Weil, David N. 2012. Measuring Economic Growth from Outer Space. *American Economic Review*, **102**(2), 994–1028.

Hodler, Roland, & Raschky, Paul A. 2014. Regional Favoritism. *The Quarterly Journal of Economics*, **129**(2), 995–1033.

Holden, Z. A., Smith, A. M. S., Morgan, P., Rollins, M. G., & Gessler, P. E. 2005. Evaluation of novel thermally enhanced spectral indices for mapping fire perimeters and comparisons with fire atlas data. *International Journal of Remote Sensing*, **26**(21), 4801–4808.

Jaiswal, K.S., & Wald, D.J. 2008. *Creating a global building inventory for earthquake loss assessment and risk management: U.S. Geological Survey Open-File Report 2008-1160.* Tech. rept. USGS.

Joyce, K. E., Belliss, S. E., Samsonov, S. V., McNeill, S. J., & Glassey, P. J. 2009. A review of the status of satellite remote sensing and image processing techniques for mapping natural hazards and disasters. *Progress in Physical Geography*, **33**(2), 183–207.

Klemas, Victor V. 2009. The Role of Remote Sensing in Predicting and Determining Coastal Storm Impacts. *Journal of Coastal Research*, **256**(nov), 1264–1275.

Knebl, M.R., Yang, Z.-L., Hutchison, K., & Maidment, D.R. 2005. Regional scale flood modeling using NEXRAD rainfall, GIS, and HEC-HMS/RAS: a case study for the San Antonio River Basin Summer 2002 storm event. *Journal of Environmental Management*, **75**(4), 325–336.

Kreibich, H., Piroth, K., Seifert, I., Maiwald, H., Kunert, U., Schwarz, J., Merz, B., & Thieken, A. H. 2009. Is flow velocity a significant parameter in flood damage modelling? *Natural Hazards and Earth System Sciences*, **9**(5), 1679–1692.

Krotkov, Nickolay A., & Li, Can. 2006. *OMI/Aura Sulphur Dioxide (SO2) Total Column 1-orbit L2 Swath 13x24 km V003, Greenbelt, MD, USA, Goddard Earth Sciences Data and Information Services Center (GES DISC), , Accessed 30 August 2016.*

Li, Xi, Xu, Huimin, Chen, Xiaoling, & Li, Chang. 2013. Potential of NPP-VIIRS Nighttime Light Imagery for Modeling the Regional Economy of China. *Remote Sensing*, **5**(6), 3057–3081.

Linkimer, Lepolt. 2007. Relationship between peak ground acceleration and Modified Mercalli intensity in Costa Rica. *Revista Geológica de América Central.*

Mati, Bancy M., Mutie, Simon, Gadain, Hussein, Home, Patrick, & Mtalo, Felix. 2008. Impacts of land-use/cover changes on the hydrology of the transboundary Mara River, Kenya/Tanzania. *Lakes & Reservoirs: Research & Management*, **13**(2), 169–177.

Merz, B., Kreibich, H., Schwarze, R., & Thieken, A. 2010. Review article "Assessment of economic flood damage". *Natural Hazards and Earth System Sciences*, **10**(8), 1697–1724.

Michalopoulos, Stelios, & Papaioannou, Elias. 2014. National Institutions and Subnational Development in Africa. *The Quarterly Journal of Economics*, **129**(1), 151–213.

Murphy, J. R., & O'Brien, L. J. 1977. The correlation of peak ground acceleration amplitude with seismic intensity and other physical parameters. *Bulletin of the Seismological Society of America*, **67**(3), 877–915.

Myint, S. W., Yuan, M., Cerveny, R. S., & Giri, C. 2008. Categorizing natural disaster damage assessment using satellite-based geospatial techniques. *Natural Hazards and Earth System Science*, **8**(4), 707–719.

National Disaster Management Agency, BNPB. 2016. *DiBi database (Data and Information on Disaster in Indonesia).*

Nichol, Janet E., Shaker, Ahmed, & Wong, Man-Sing. 2006. Application of high-resolution stereo satellite images to detailed landslide hazard assessment. *Geomorphology*, **76**(1-2), 68–75.

OMI team. 2012. *Ozone Monitoring Instrument (OMI) Data Users Guide.* User Manual. OMI.

Penning-Rowsell, Edmund, Johnson, Clare, Tunstall, Sylvia, Tapsell, Sue, Morris, Joe, Chatterton, John, & Green, Colin. 2005. *The benefits of flood and coastal risk management: a handbook of assessment techniques.* Tech. rept. Middlesex University Press.

Raschky, Paul A. 2013. *Discussion Paper: Estimating the Effects of West Sumatra Public Asset Insurance Program on Short-Term Recovery after the September 2009 Earthquake.* Tech. rept. 2013-35. ERIA.

Römer, H., Willroth, P., Kaiser, G., Vafeidis, A. T., Ludwig, R., Sterr, H., & Diez, J. Revilla. 2012. Potential of remote sensing techniques for tsunami hazard and vulnerability analysis – a case study from Phang-Nga province, Thailand. *Natural Hazards and Earth System Science*, **12**(6), 2103–2126.

Roy, D.P., Boschetti, L., & Trigg, S.N. 2006. Remote Sensing of Fire Severity: Assessing the Performance of the Normalized Burn Ratio. *IEEE Geoscience and Remote Sensing Letters*, **3**(1), 112–116.

Scawthorn, Charles, Flores, Paul, Blais, Neil, Seligson, Hope, Tate, Eric, Chang, Stephanie, Mifflin, Edward, Thomas, Will, Murphy, James, Jones, Christopher, *et al.* 2006. HAZUS-MH flood loss estimation methodology. II. Damage and loss assessment. *Natural Hazards Review*, **7**(2), 72–81.

Shi, Kaifang, Yu, Bailang, Huang, Yixiu, Hu, Yingjie, Yin, Bing, Chen, Zuoqi, Chen, Liujia, & Wu, Jianping. 2014. Evaluating the Ability of NPP-VIIRS Nighttime Light Data to Estimate the Gross Domestic Product and the Electric Power Consumption of China at Multiple Scales: A Comparison with DMSP-OLS Data. *Remote Sensing*, **6**(2), 1705–1724.

Shrestha, M.S., Artan, G.A., Bajracharya, S.R., Gautam, D.K., & Tokar, S.A. 2011. Bias-adjusted satellite-based rainfall estimates for predicting floods: Narayani Basin. *Journal of Flood Risk Management*, **4**(4), 360–373.

Skoufias, Emmanuel, Strobl, Eric, & Tveit, Thomas. 2017. The Reallocation of District-Level Spending and Natural Disasters: Evidence from Indonesia. *World Bank Policy Research Working Paper (Forthcoming).*

Sun, Donglian, Li, Sanmei, Zheng, Wei, Croitoru, Arie, Stefanidis, Anthony, & Goldberg, Mitchell. 2015. Mapping floods due to Hurricane Sandy using NPP VIIRS and ATMS data and geotagged Flickr imagery. *International Journal of Digital Earth*, **9**(5), 427–441.

The Atlantic. 2014 (December). *Ten Years Since the 2004 Indian Ocean Tsunami.*

The Global Facility for Disaster Reduction and Recovery. 2011. *Indonesia: Advancing a National Disaster Risk Financing Strategy Options for Consideration.* Report. World Bank.

Tralli, David M., Blom, Ronald G., Zlotnicki, Victor, Donnellan, Andrea, & Evans, Diane L. 2005. Satellite remote sensing of earthquake, volcano, flood, landslide and coastal inundation hazards. *ISPRS Journal of Photogrammetry and Remote Sensing*, **59**(4), 185–198.

Wald, David J., Quitoriano, Vincent, Heaton, Thomas H., Kanamori, Hiroo, Scrivner, Craig W., & Worden, C. Bruce. 1999. TriNet ShakeMaps: Rapid Generation of Peak Ground Motion and Intensity Maps for Earthquakes in Southern California. *Earthquake Spectra*, **15**(3), 537–555.

Wald, D.J., Worden, B.C., Quitoriano, V., & Pankow, K.L. 2005. *ShakeMap Manual - Technical Manual, User's Guide, and Software Guide.* Technical Manual. USGS.

World Bank. 2005 (January). *Indonesia: Preliminary Damage and Loss Assessment: The December 26, 2004 Natural Disaster.*

Wu, Huan, Adler, Robert F., Hong, Yang, Tian, Yudong, & Policelli, Fritz. 2012. Evaluation of Global Flood Detection Using Satellite-Based Rainfall and a Hydrologic Model. *Journal of Hydrometeorology*, **13**(4), 1268–1284.

Wu, Huan, Adler, Robert F., Tian, Yudong, Huffman, George J., Li, Hongyi, & Wang, JianJian. 2014. Real-time global flood estimation using satellite-based precipitation and a coupled land surface and routing model. *Water Resources Research*, **50**(3), 2693–2717.

Yamazaki, Fumio, & Matsuoka, Masashi. 2007. Remote Sensing Technologies in Post Disaster Damage Assessment. *Journal of Earthquake and Tsunami*, **01**(03), 193–210.